

A modified surface charge approach to the film growth and dissolution of iron in concentrated phosphoric acid

Iva Betova

Received: 19 November 2014 / Revised: 29 January 2015 / Accepted: 29 January 2015 / Published online: 10 March 2015
© Springer-Verlag Berlin Heidelberg 2015

Abstract Rotating ring-disk voltammetric, photo-electrochemical, and impedance measurements were performed to study the film growth and dissolution of iron in concentrated H_3PO_4 . The only species released in the current plateau region is Fe(III), and its release consumes ca. 90 % of the total current passing through the disk. This means that most of the charge passed is consumed for the dissolution of Fe through the oxide film, and the film formation efficiency is very low. Photocurrent spectroscopy allows the identification of the anodic layer with doped ferric oxide. Potential dependence of photocurrent is governed by a Poole-Frenkel mechanism of electronic carrier generation. An updated version of the so-called surface charge approach to the mechanism of conduction of anodic oxide films is proposed to explain the obtained impedance spectra. It is based on the assumptions that interstitial cations are the main ionic charge carriers and that the field strength in the barrier layer is constant. A negative surface charge built up at the film/solution interface via accumulation of cation vacancies accelerates interstitial cation transport, thus explaining the pseudo-inductive behavior of the iron/film/electrolyte system under small amplitude perturbation.

Keywords Iron · Fe(II)/Fe(III) oxide · Phosphoric acid · Electrochemical impedance spectroscopy · Kinetic model

Introduction

The understanding of the passivity of metals requires the establishment of a quantitative correlation between the defect

structure of anodic oxide films and the transport rates of mobile species in such films. Particularly so, because of the fact that film growth and dissolution of the metal through the passive layer are thought to be largely determined by point defect transport.

In the contemporary models for the passive state, it is usually assumed that the point defects in the oxygen and cation sub-lattices of the oxide are transported independently of each other [1–4]. During the growth of a continuous barrier-like layer on an anodically polarized metal, it is universally accepted that the generation and consumption of point defects whose transport is responsible for film growth occurs at the interfaces with the substrate metal and the electrolyte solution [2–4]. However, far less attention has been paid to the kinetics of the interfacial electrochemical reactions of defect generation and consumption in comparison with the transport mechanism in the passive film itself [2–5]. Consequently, the possibility of defect interaction at the interfaces or in the near-interface layers has seldom been taken into account. This is surprising since if the steady-state rates of defect transport are much slower than the rates of defect generation and consumption, defects accumulate in the interfacial regions. In other words, the probability of a defect interaction process is highest close to the interfaces.

Transient phenomena in metal/barrier oxide film/electrolyte systems have been extensively studied in order to get deeper insight into the mechanism of film growth and the kinetics of relaxation processes [6–24]. For a range of metals in the passive state, a current or potential “overshoot” is observed in potentiostatic and galvanostatic transients or a pseudo-inductive behavior appears in the impedance spectra [6–24]. The essential electric equivalence between these types of transient behavior has been demonstrated [6–8, 19, 20, 25, 26], and it has been suggested that the transport of two charge carrier species in a semi-insulating medium can give rise to such a transient phenomenon [25, 26]. In general, if one of the

I. Betova (✉)
Department of Chemistry, Technical University of Sofia, Kliment
Ohridski Boulevard 8, 1000 Sofia, Bulgaria
e-mail: iva_betova@tu-sofia.bg

charges is injected at the metal/film interface, the corresponding partial current will be limited by the space charge formed. This situation may be relieved by the injection of a certain charge of opposite polarity from the electrolyte. The time delay of the rising current (or the characteristic frequency of the pseudo-inductive loop) is thought to be essentially determined by the time elapsed until the opposite charges compensate the space charge formed. In other words, the increase of differential conductivity of the metal/oxide film/electrolyte system during the transient until further film growth is governed by a charge compensation mechanism.

A few years ago, a report attempting at explaining such a behavior in terms of the interaction between point defects of opposite sign at the film/solution interface in the transient regime was published [27]. The chemistry of the Point Defect Model and most of its basic assumptions [2, 3] were used to derive a quantitative model able to reproduce the experimentally observed pseudo-inductive behavior in the impedance spectra [27]. Further, this model was coupled to a set of interfacial reactions in order to reproduce such a behavior during transpassive dissolution of Fe-Cr alloys [28] and very recently the active-to-passive transition of Nb, Mo, W, and Ti [29–34].

In all these cases, it was assumed that oxygen vacancies are the main ionic current carriers and that their transport, giving rise to film growth, is accelerated in the transient regime via interaction with cation vacancies resulting in a charge compensation mechanism. However, the well-known case of the passive film on Fe cannot be rationalized on such a basis since it has been demonstrated that the film has an inverse spinel-like structure [35] in which interstitial cations are the major and cation vacancies the minor ionic current carriers [5]. In addition, transient effects such as an overshoot in a galvanostatic or potentiostatic transient or pseudo-inductive behavior in the impedance spectra for passive Fe have been reported a number of times [1, 11, 14, 15]. Very recently, some of us proposed a model for the passivation of Fe in 14.8 M H_3PO_4 [36] in which a formation of a Fe(III)-based film was assumed to compete with dissolution of both divalent and trivalent Fe. No detailed mechanism for the dissolution of Fe(III) through the film was devised within the framework of this model, and thus, it cannot be considered valid in the situation in which the thickness of the oxide film exceeds a few monolayers.

The purpose of the present paper is to propose a modified surface charge approach that is able to account quantitatively for the film growth and dissolution of Fe in 14.8 M H_3PO_4 . First, rotating ring-disk electrode voltammetric, photo-electrochemical, and impedance measurements on Fe are presented and discussed. Second, the physico-chemical basis of a modified surface charge approach is described emphasizing the particular point defect structure of the oxide film on Fe and the kinetics of the interfacial reactions involved in the change of the film stoichiometry. Next, the relevant equations to formulate a quantitative model are briefly introduced. Finally, the

relevance of kinetic parameters derived from the calculation procedure to the film growth and dissolution on Fe is outlined and some limitations of the model approach are indicated.

Materials and methods

For the voltammetric, impedance, and rotating ring-disk studies, electrodes featuring an Fe disk (99.95 %, Goodfellow, exposed area 0.16 cm^2) and a ring made of Au (99.9 %, ring area 0.1 cm^2) were employed. The theoretical collection efficiency $N_t=0.32$ of the ring-disk electrode arrangement was verified experimentally using an Au-disk/Au-ring electrode with the same geometry in a solution containing the $\text{K}_3\text{Fe}(\text{CN})_6$ - $\text{K}_4\text{Fe}(\text{CN})_6$ redox couple. An Fe disk insulated with protective varnish, molded in epoxy resin, and inserted in a polytetrafluorethene (PTFE) holder to expose 0.2 cm^2 to the electrolyte was used in the photo-electrochemical measurements. The electrode pre-treatment consisted of mechanical polishing with emery papers of grade 600 to 4000, degreasing with acetone, rinsing with distilled water, and pre-polarization in the hydrogen evolution region for the removal of the air-formed film. A conventional three-electrode cell featuring a Pt counter electrode and Hg/ Hg_2SO_4 /sat. K_2SO_4 reference electrode ($E_{\text{SHE}}=0.66 \text{ V}$) was employed. All the potentials are expressed vs. the standard hydrogen electrode (SHE). Reagent grade 85 % H_3PO_4 (14.8 M) served as the electrolyte and was used as received. All the measurements were carried out at room temperature ($20 \pm 1 \text{ }^\circ\text{C}$) in a solution deaerated with Ar (99.995 %).

The voltammetric, impedance spectroscopic and rotating ring-disk measurements were performed with an Autolab[®] PGSTAT20 (Eco Chemie B.V.) potentiostat equipped with a bi-potentiostat and frequency response analyzer modules and driven by GPES 4.6 and FRA 4.6 software (Eco Chemie B.V.). The frequency range was typically between 0.01 Hz and 30 kHz at an AC signal amplitude of 10 mV (rms), whereas the rotation rates ranged between 300 and 1200 rpm. The reproducibility of the impedance spectra was $\pm 2 \%$ by amplitude and $\pm 3^\circ$ by phase shift. The validation of the impedance spectra was performed by checking the linearity condition, i.e., measuring spectra at AC signal amplitudes between 2 and 20 mV (rms), and the causality by a Kramers-Kronig compatibility test. An Oriel 300 W Xe-lamp combined with an Oriel Multispec 257 monochromator and a mechanical chopper (Bentham model 218) was used as a modulated light source in photocurrent measurements (wavelength 300–700 nm, modulation frequency 10–300 Hz). The photocurrent was registered by a PAR 5210 lock-in amplifier coupled to a PAR 283 potentiostat. Quantum efficiencies were calculated by correcting the measured photocurrent for the spectral dependence of the lamp-monochromator light power measured by an optical power meter (Graseby Optronics). The

reflections at the metal/film interface were not taken into account. Simulation and non-linear least squares fitting of steady-state current vs. potential curves and impedance spectra to the equations of the proposed model were performed using Originlab software.

Results

Relative importance of different processes on Fe in 14.8 M H₃PO₄

Figure 1a shows a linear sweep voltammogram of Fe in 14.8 M H₃PO₄ (rotation rate 1200 rpm, sweep rate 10 mV s⁻¹) together with the detection of released Fe(II) by its oxidation at the Au ring to Fe(III) ($E_{ring}=1.14$ V) as well as the detection of released Fe(III) by its reduction at the Au ring to Fe(II) ($E_{ring}=-0.06$ V). The ring currents were normalized, taking into account the theoretical collection efficiency and the difference in the number of electrons transferred in the overall disk and ring reactions. A quantitative kinetic model

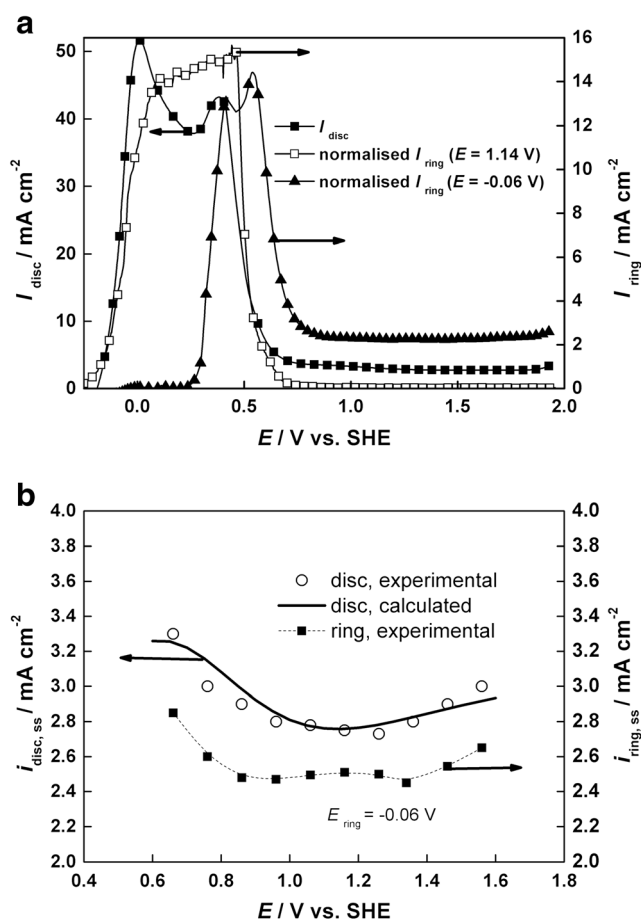


Fig. 1 a Disk current vs. potential (left) and normalized ring currents vs. potential (right) for ring potentials of 0.06 and 1.14 V, rotation speed of 1200 rpm, and sweep rate of 10 mV s⁻¹; b steady-state disk and ring currents vs. potential in the plateau region (0.6–1.6 V)

of the processes in the pre-passive dissolution and passivation regions (−0.2 to 0.7 V) was proposed and tested vs. experimental results in previous work [31]. Focusing on the current plateau region (0.7–1.8 V), the current is not significantly dependent on potential, preserving a relatively high value of ca. 3 mA cm⁻². The values of the steady-state disk current, measured at rotation rates from 300 to 1800 rpm by a 30-min polarization at each potential in the plateau region, are shown in Fig. 1b and were found to coincide with the voltammetric disk current within the experimental error. This means that the steady-state current in the plateau region is independent of potential, rotation rate, and sweep rate. The only species released in this region is Fe(III), and its release consumes ca. 90 % of the total current passing through the disk. The value of the ring current for the reduction of Fe(III) to Fe(II) is also independent of the sweep rate and coincides with the ring current measured via potentiostatic polarization (Fig. 1a, b). This means that most of the charge passed is consumed for the dissolution of Fe through the oxide film, and the film formation efficiency is very low. Such a low efficiency can be explained by a fast dissolution rate of the oxide in 14.8 M H₃PO₄ and is in accordance with earlier results of other authors [14, 15].

Electronic properties of the oxide film on Fe in 14.8 M H₃PO₄

To assess the electronic properties of the oxide film, photoelectrochemical measurements were used. A light modulation frequency of 205 Hz (close to which the photocurrent is in phase with the optical excitation, i.e., is at its maximum) was employed in order to minimize the effect of ionic processes on the photo-electrochemical response. Figure 2 presents spectra of the incident photon to photocurrent conversion efficiency (IPCE) for Fe in 14.8 M H₃PO₄ measured in the plateau region (1.3–1.9 V). The spectra are analogous to those published by a range of authors for passive Fe in different electrolytes [4, 37–40]. Assuming non-direct transitions through the optical band gap, plots of the square root of the quantum efficiency

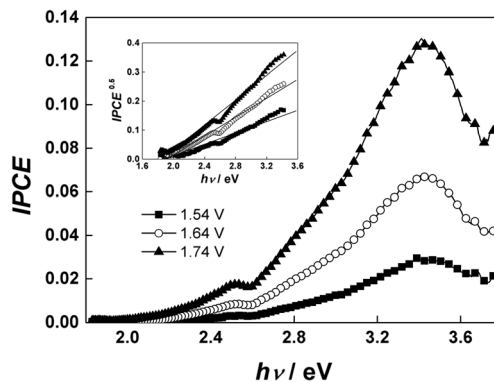


Fig. 2 Incident photon to photocurrent conversion efficiency vs. photon energy for the oxide film on Fe in 14.8 M H₃PO₄ at three potentials. Inset determination of the optical band gap for an indirect transition

vs. photon energy are shown in the insert of the figure. The energy axis intercept furnishes an estimate of the optical band gap of 1.85 eV regardless of the potential, in qualitative agreement with earlier results [4, 37–42].

The dependencies of the quantum efficiency on potential measured at different photon energies are shown in Fig. 3. The form of the curves is similar regardless of the photon energy and analogous to those published by other authors for different electrolytes [39–42]. A quasi-exponential increase of the quantum efficiency is observed in the potential range 1.2–1.8 V. Such an exponential increase suggests the validity of a Poole-Frenkel mechanism for the photocurrent generation. Assuming that the space charge layer thickness associated with electron donors is smaller than the film thickness, Eq. (1) for the quantum efficiency applies,

$$\text{IPCE} = A \exp \left[\sqrt{\frac{e^3}{\pi \epsilon \epsilon_0}} \left(\frac{e N_D}{2 \epsilon \epsilon_0} \right)^{0.25} \frac{(E - E_{fb})^{0.25}}{kT} \right] \quad (1)$$

where A is a constant depending on the photon energy. Using the flat-band potential estimated on the basis of the high-frequency capacitance of the film (see below), semi-logarithmic plots of IPCE vs. $(E - E_{fb})^{0.25}$ were constructed and are shown in the insert of Fig. 3. These plots are linear to a first approximation, and their slopes do not depend on photon energy within the experimental error. The value of the slope can be used to extract an estimate of the donor density $N_D = 3.1 \times 10^{21} \text{ cm}^{-3}$ if a value of 15 is tentatively assumed for the dielectric constant of the oxide.

The ionic conduction process in the oxide film on Fe in 14.8 M H_3PO_4

Impedance spectroscopic measurements were applied to gather information on the ionic conduction process in the anodic oxide film of Fe in 14.8 M H_3PO_4 . Figure 4 presents the

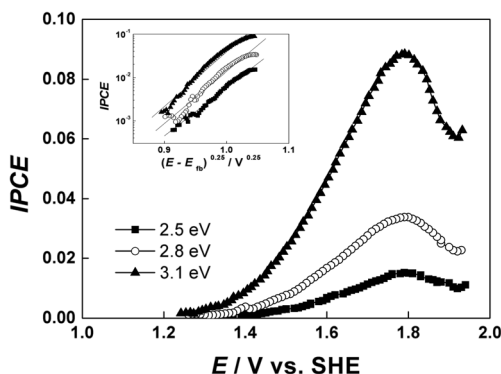


Fig. 3 Incident photon to photocurrent conversion efficiency vs. potential at three photon energies for the oxide film on Fe in 14.8 M H_3PO_4 . *Inset* Poole-Frenkel representation of the IPCE

resulting impedance spectra at three potentials in the plateau region (rotation rate 600 rpm). It is noteworthy to mention that the rotation rate does not have any measurable effect on the impedance spectra, i.e., solution transport is most probably not a rate-determining step of the overall reaction in this region. The spectra are qualitatively analogous to those published earlier for Fe in 1 M H_2SO_4 and H_3PO_4 solutions [14, 15], and to the spectra registered for a range of other metals in the passive state [9, 16, 18, 19, 21–23, 27, 29–34]. The identification of the observed time constants can be stated as follows [27]. The high-frequency time constant is associated with the parallel combination of the capacitance of the depletion layer and the resistance due to point defect migration through it, whereas the pseudo-inductive time constant—with surface charge compensation accelerating the migration of point defects. An extra capacitive time constant observed in the frequency range 1–10 Hz can be tentatively identified with an interfacial charge transfer reaction. The negative low-frequency impedance observed at 0.76 V is in good agreement with the negative slope of the steady-state current vs. potential curve in this potential region (Fig. 1b) and is most probably related to the gradual coverage of the surface with Fe(III) oxide.

The high-frequency capacitance C_{hf} calculated from the impedance spectra obeys to a first approximation a Mott-Schottky dependence on potential (Fig. 5). This is in good accordance with the semi-conductor properties of the oxide film on Fe. The slope of the C_{hf}^{-2} vs. E dependence confirmed the value of the donor density estimated from the photocurrent vs. potential curve (insert of Fig. 3). On the other hand, the intercept gives an estimate for the flat-band potential $E_{fb} = 0.56$ V. This value was used above in the numerical processing of the photocurrent voltammograms. The estimates for N_D obtained from the photocurrent and high-frequency capacitance are in good agreement with each other. On the other hand, the linear dependence of the product $R_{hf} i_{ss}$, where R_{hf} is the resistance associated with the high-frequency loop and i_{ss} the steady-state current density, suggests the validity of a high-field migration mechanism as pointed out already by Keddad et al. [14] for Fe in H_2SO_4 and H_3PO_4 solutions.

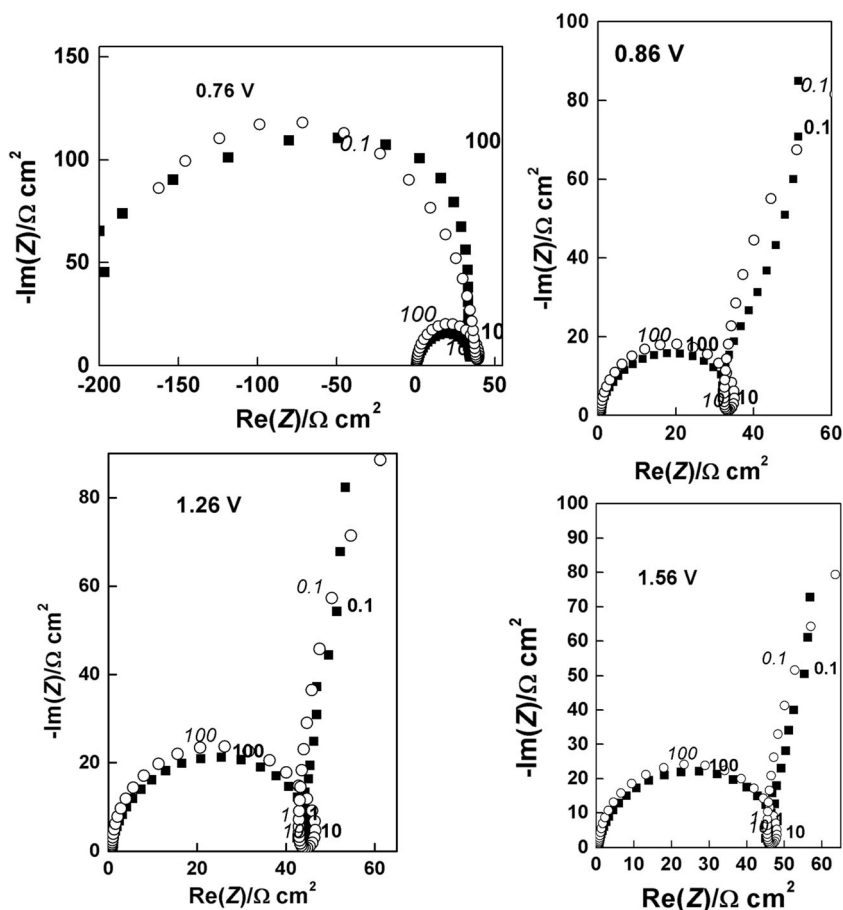
Discussion

Reaction model

In this section, a modified surface charge approach that is able to explain the reaction dynamics of Fe in 14.8 M H_3PO_4 is proposed. Recent work of Bojinov and co-workers on the passivation of Nb, W, and Ti was used as the model framework [29–34].

Following the recent extensive structural investigations of the passive film on Fe in different media [35, 43–45], it can be

Fig. 4 Electrochemical impedance spectra in the plateau region of Fe in 14.8 M H₃PO₄. Closed symbols experimental data, open symbols best-fit calculation. Parameter is frequency in hertz



assumed that it has a nano-crystalline inverse spinel structure with a certain concentration of mobile interstitial cations and cation vacancies. It is further proposed that mobile interstitial cations are divalent, Fe_i²⁺, whereas cation vacancies are trivalent, V_{Fe}³⁺. The solid state growth mechanism of such films implies a certain concentration of oxygen vacancies as well [2–5]. However, they are assumed to play a minor role in the defect structure at steady state. In other words, dissolution of

Fe through the film takes place in such a state, the film growth being neglected as a slow parallel reaction. This fact is in accordance with the suggestions of several authors [11, 14, 15] and in agreement with the RRD experiments performed in the present work that clearly demonstrate that trivalent iron dissolution through the film is the main process taking place in the plateau region. In what follows, iron dissolution is assumed to proceed via two parallel routes. The first route involves the consumption of interstitial cations at the film/solution interface:

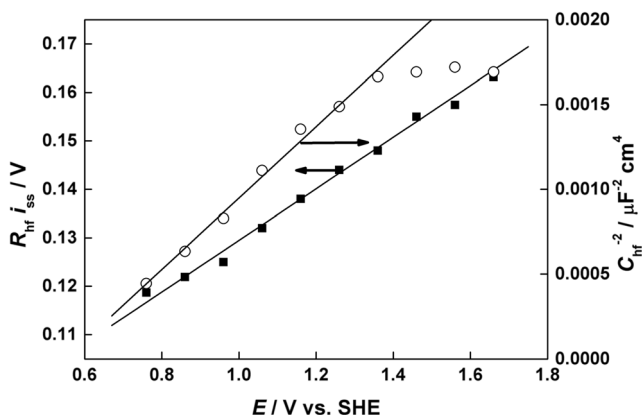


Fig. 5 Product of the resistance of the high-frequency loop and the current density (left axis) and high-frequency capacitance in Mott-Schottky coordinates (right axis)



In this notation, Fe_{Fe}^{III*} represents a trivalent iron cation produced by oxidation of a divalent interstitial cation at the interface. It is supposed to be associated with a phosphate ion.

The interstitial cations are generated by the oxidation reaction at the metal/film interface



They are transported through the film by a high-field migration mechanism accelerated by the surface charge of cation vacancies in analogy with the surface charge approach

$$J_i = \frac{D_i c_i(L)}{2a} \exp \left\{ \frac{2Fa}{RTL} \left[(1-\alpha)E + \frac{4FL_{F/S}^2}{\varepsilon\varepsilon_0} c_{V_{Fe}'''}(0) \right] \right\} \quad (6)$$

Another route of dissolution of iron proceeds via the generation of iron cation vacancies at the film/solution interface.



Since no transfer of electrons takes place in this step, it is considered to be purely chemical in nature, i.e., independent of the applied potential.

Cation vacancies are transported through the film by a high-field migration

$$J_v = \frac{D_v c_v(0)}{2a} \exp \left\{ \frac{3Fa}{RTL} (1-\alpha)E \right\} \quad (8)$$

and consumed at the metal/film interface.



In Eqs. (7) and (9), Fe_{Fe}^{III} represents an ordinary trivalent iron cation in the oxide lattice. In writing Eq. (8), it is assumed that the transport of cation vacancies is not influenced by the surface charge of these vacancies, in analogy with a previous paper [13].

Following the above assumptions, the faradaic current density in the system is the sum of the partial current densities due to the motion of interstitial cations and cation vacancies.

$$I_F = I_i + I_v \quad (10)$$

The current density due to interstitial cations is given by the following charge balance

$$\frac{I_i}{3F} = J_i = k_2 \gamma_{II} + k_{32} \gamma_{III}^* \quad (11)$$

where γ_{II} and γ_{III}^* are the fractions of the F/S interface occupied by $Fe_i^{\cdot\cdot}$ and Fe_{Fe}^{III*} , respectively, referred to the cation sub-

lattice only. A charge of three electrons is considered for each interstitial cation since Fe dissolves as $Fe(III)$ in the plateau region; in this way, the flux of electrons, from the F/S interface where they are generated by reactions (2) and (3) to the metal, is taken into account.

In turn, the current density due to cation vacancies can be expressed as

$$\frac{I_v}{3F} = J_v = k_{33} \gamma_{III} \quad (12)$$

where γ_{III} is the fraction at the F/S interface occupied by Fe_{Fe}^{III} positions.

The material balances of the $Fe_i^{\cdot\cdot}$ and Fe_{Fe}^{III*} positions in the outermost cation layer are written as

$$\frac{\beta d\gamma_{II}}{dt} = \frac{I_i}{3F} - k_2 \gamma_{II} - k_{31} \gamma_{II} \quad (13)$$

$$\frac{\beta d\gamma_{III}^*}{dt} = k_{31} \gamma_{II} - k_{32} \gamma_{III}^* \quad (14)$$

In these equations, the constant β corresponds to the total number of cation positions per unit surface in that layer.

Steady-state solution

In the steady state, Eqs. (13) and (14) become

$$0 = \frac{\bar{I}_i}{3F} - \bar{k}_2 \bar{\gamma}_{II} - \bar{k}_{31} \bar{\gamma}_{II} \quad (15)$$

$$0 = k_{32} \bar{\gamma}_{III}^* - \bar{k}_{31} \bar{\gamma}_{II} \quad (16)$$

where steady-state values of variables are marked with an overline. It is to be noted that Eq. (16) is the sum of Eqs. (11) and (15).

The sum of all steady-state surface fractions in the outermost cation layer must be equal to 1, i.e.,

$$\bar{\gamma}_{II} + \bar{\gamma}_{III}^* + \bar{\gamma}_{III} = 1 \quad (17)$$

where $\bar{\gamma}_{III}$ is the surface fraction occupied by regular Fe_{Fe}^{III} sites, at which dissolution of iron mediated by cation vacancies (Eq. 9) takes place.

The steady-state current density due to interstitial cations can be calculated from Eqs. (11), (15), and (16) as

$$\bar{I}_i = \frac{3Fk_{32}(\bar{k}_2 + \bar{k}_{31})}{\bar{k}_{31} + k_{32}}(1 - \bar{\gamma}_{III}) = 3F\bar{k}_i(1 - \bar{\gamma}_{III}) \tag{18}$$

whereas the steady-state current density due to cation vacancies is defined as

$$I_V = 3Fk_{33}\bar{\gamma}_{III} \tag{19}$$

If $\bar{\gamma}_{III}$ is defined as a function of the reaction rates for the formation of interstitial cations and cation vacancies, i.e.,

$$\bar{\gamma}_{III} = \frac{k_{33}}{\bar{k}_i + k_{33}} \tag{20}$$

the following expressions for the partial current densities are obtained:

$$\bar{I}_i = \frac{3F\bar{k}_i^2}{\bar{k}_i + k_{33}} \tag{21}$$

$$\bar{I}_V = \frac{3Fk_{33}^2}{\bar{k}_i + k_{33}} \tag{22}$$

The steady-state current vs. potential curve calculated by the sum of Eqs. (21) and (22) and by appropriate choice of fitting parameters is shown in Fig. 1b with a solid line. In the calculations, the rate constants of electron transfer reactions at the film/electrolyte interface were assumed to be exponential functions of E : $k_i = k_i^0 \exp(b_i E)$, with the b_i coefficients expressed by $b_i = \frac{\alpha_i n F}{RT}$, where α_i is the usual transfer coefficient. Figure 1b demonstrates that the agreement between the calculated curve and the experimental points is satisfactory, demonstrating the feasibility of the proposed model.

Small amplitude alternating current solution

In agreement with Eq. (10), which assumes that currents transported by interstitial cations and cation vacancies are additive, and taking into account capacitive phenomena, the impedance of the system is defined as the parallel combination of the impedance due to generation and transport of cation vacancies (Z_V), the impedance due to transport and consumption of interstitial cations (Z_i), and the impedance due to the capacitance of the depletion layer in the semi-conductor oxide.

$$Z = \left[\frac{j\omega}{C_{sc}^{-1}} + \frac{1}{Z_i} + \frac{1}{Z_V} \right]^{-1} \tag{23}$$

Impedance due to generation and transport of cation vacancies

This impedance is represented by a migration resistance

$$Z_v^{-1} = \frac{4F\bar{I}_v a E / RT}{\bar{E}(1 - \alpha)} \tag{24}$$

Impedance due to transport and consumption of interstitial cations

In analogy with the surface charge approach [13], the impedance due to transport of interstitial cations is given by

$$Z_{i,f}^{-1} = \frac{2F\bar{I}_i a E / RT}{\bar{E}} \left[1 + \frac{\alpha}{(1 - \alpha) \left(j\omega \frac{1}{\bar{I}_i S} + 1 \right)} \right] \tag{25}$$

where S is the capture cross section of positively charged interstitial cations by negative surface charges (cation vacancies) at the F/S interface. This impedance corresponds to an inductive loop.

The faradaic impedance for the consumption of interstitial cations at the F/S interface is derived from Eq. (11).

$$Z_{i,F/S}^{-1} = 3F \left(\tilde{k}_2 \tilde{\gamma}_{II} + \bar{k}_2 \tilde{\gamma}_{II} + k_{32} \tilde{\gamma}_{III}^* \right) \tag{26}$$

where derivatives of variables with respect to potential are marked with the tilde sign. The variations of $\tilde{\gamma}_{II}$ and $\tilde{\gamma}_{III}^*$ are obtained from the mass balance Eqs. (13) and (14) which, written under small amplitude sine wave perturbation conditions, become

$$\beta j\omega \tilde{\gamma}_{II} = \frac{Z_{i,F/S}^{-1}}{3F} - \tilde{k}_2 \tilde{\gamma}_{II} - \bar{k}_2 \tilde{\gamma}_{II} - \tilde{k}_{31} \tilde{\gamma}_{II} - \bar{k}_{31} \tilde{\gamma}_{II} \tag{27}$$

$$\beta j\omega \tilde{\gamma}_{III}^* = \tilde{k}_{31} \tilde{\gamma}_{II} + \bar{k}_{31} \tilde{\gamma}_{II} - k_{32} \tilde{\gamma}_{III}^* \tag{28}$$

Solving Eqs. (27) and (28) for the surface fractions and inserting the result in Eq. (26) leads to

$$Z_{i,F/S} = R_t \left[1 + \frac{b_{31} \bar{k}_{31} (\bar{k}_2 - \bar{k}_{31})}{\left(1 + j \frac{\omega}{\omega^*}\right) (b_2 \bar{k}_2 k_{32} + b_{31} \bar{k}_{31}^2 + \bar{k}_{31} \bar{k}_2 (b_2 - b_{31}))} \right] \quad (29)$$

with

$$R_t^{-1} = 3Fb_2 \bar{k}_2 \bar{\gamma}_{II} \quad (30)$$

and

$$\omega^* = \frac{b_2 k_{32} \bar{k}_2 + b_{31} \bar{k}_{31}^2}{\beta \bar{k}_2 b_2} \quad (31)$$

Thus, the overall impedance due to generation and transport of interstitial cations, Z_i , is given by

$$Z_i = Z_{i,f} + Z_{i,F/S} \quad (32)$$

The impedance spectra in the potential interval 0.7–1.6 V were fitted to the transfer function defined by Eqs. (23)–(32) in order to obtain the values of the kinetic parameters. The fitted impedance spectra are shown in Fig. 4 with open symbols and demonstrate the ability of the model to account for the impedance response as well.

The parameters determined from the fitting procedure are listed in Table 1. The steady-state fractions of $\text{Fe}_{\text{Fe}}^{\text{III}}$ and $\text{Fe}_{\text{Fe}}^{\text{III}*}$ at the film/electrolyte interface calculated from the model are presented in Fig. 6 as a function of the applied potential. From the obtained estimates, it is clear that the main species at the film/electrolyte interface are $\text{Fe}_{\text{Fe}}^{\text{III}}$ and $\text{Fe}_{\text{Fe}}^{\text{III}*}$ which is in good

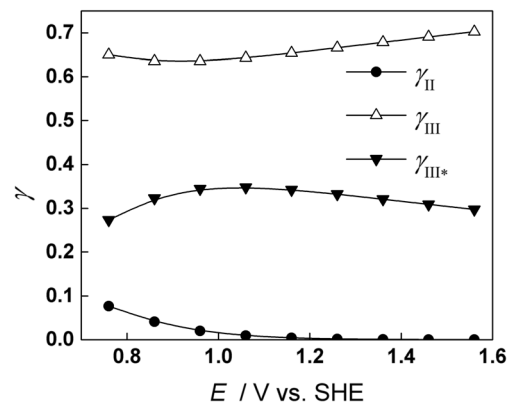


Fig. 6 Steady-state fractions of Fe_i^{I} , $\text{Fe}_{\text{Fe}}^{\text{III}}$, and $\text{Fe}_{\text{Fe}}^{\text{III}*}$ calculated by the model depending on the applied potential

agreement with the ring-disk results demonstrating that Fe dissolves only as Fe(III) in the plateau region. The main dissolution route is via the reaction sequence (7)–(9), and the secondary dissolution route is via reactions (2)–(4). This means that the concentration of interstitial cations in the oxide is larger than that of cation vacancies, since the rate of consumption of interstitial cations at the film/electrolyte interface is overall slower than that of generation of cation vacancies at the same interface. Since the interstitial cations are positively charged defects that can play the role of electron donors, this explains the *n*-type semi-conductor behavior of the oxide film as evidenced by the photocurrent and capacitance vs. potential measurements in the present work. It is worth mentioning that interstitial cations have been demonstrated to be the dominant defects in the passive film on Fe in recent work [46, 47]. The exponential coefficients b_2 and b_{31} have reasonable values, leading to transfer coefficients of the order of 0.3–0.4, well within the expectations of electrochemical kinetics. The electric field strength value is comparable, albeit somewhat lower than that estimated by other authors [5, 46, 47] and is within the limits of validity of the high-field approximation of the transport equations as employed in the present paper. On the other hand, the value of the half-jump distance, a , is somewhat larger than that estimated earlier for Fe in borate buffer solution [5], indicating a certain difference between the structure of the oxide films formed in neutral and strongly acidic solutions. Finally, if as in analogy with previous work [27, 30, 31, 33, 34] it is assumed that the capture cross section of a cation vacancy by an interstitial cation at the film/electrolyte interface can be expressed as $S = (F\beta_i)^{-1}$, where β_i is the surface concentration of interstitial cations; a value of 0.74 nmol cm⁻² is estimated for that concentration. This value is much smaller than the concentration of cation positions ($\beta = 32.6$ nmol cm⁻²), and thus the fact that the concentration of interstitial cations was neglected with respect to normal cation positions during the derivation of the model appears reasonable.

Table 1 Best-fit values of the kinetic parameters of the proposed model for the film growth and dissolution on Fe in 14.8 M H_3PO_4

Parameter	Value
$10^8 k_2^0 / \text{mol cm}^{-2} \text{ s}^{-1}$	1.24
$10^9 k_{31}^0 / \text{mol cm}^{-2} \text{ s}^{-1}$	2.56
$10^9 k_{32} / \text{mol cm}^{-2} \text{ s}^{-1}$	1.59
$10^8 k_{33} / \text{mol cm}^{-2} \text{ s}^{-1}$	1.26
b_2 / V^{-1}	7.1 ($\alpha_2 = 0.36$)
b_{31} / V^{-1}	7.9 ($\alpha_2 = 0.41$)
a / nm	0.39
α	0.49
E / MVcm^{-1}	1.17
$S / \text{cm}^2 \text{ mC}^{-1}$	13.9
$\beta / \text{nmol cm}^{-2}$	32.6

Conclusions

In the present work, the film growth and dissolution on iron in concentrated H_3PO_4 was studied by a combination of electrochemical and photo-electrochemical techniques. A kinetic model of the process was proposed and quantitatively compared to the steady-state current vs. potential and electrochemical impedance data in order to obtain estimates for the main parameters of the model—rate constants of reactions at the film/electrolyte interface, field strength in the oxide, activation distance, as well as surface concentrations of normal cation and interstitial cation positions. The model is based on a modified version of the surface charge approach in which recombination of Frenkel-type defects (interstitial cations and cation vacancies) is introduced instead of the more customary recombination of Schottky-type defects (cation and anion vacancies). The following conclusions can be drawn from the experimental and calculation results:

1. The steady-state current in the plateau region is almost independent of potential, rotation rate, and sweep rate. The only species released in this region is Fe(III), and its release consumes ca. 90 % of the total current passing through the disk.
2. Assuming non-direct optical transitions, an estimate of 1.85 eV is obtained for the band gap regardless of the applied potential. The photocurrent vs. potential dependence at constant wavelength was quantitatively interpreted on the basis of a Poole-Frenkel mechanism assuming that the space charge layer thickness is smaller than the film thickness. The obtained estimate of the density of donors was found to be in good agreement with the value obtained from capacitance vs. potential measurements ($3 \times 10^{21} \text{ cm}^{-3}$).
3. The impedance spectra were somewhat analogous to those obtained for a range of metals in acidic solutions and were interpreted on the basis of the surface charge approach. Based on this approach, the high-frequency time constant was associated with the parallel combination of the capacitance of the depletion layer and the resistance due point defect migration through it. On the other hand, the pseudo-inductive time constant was related to the contribution of the surface charge compensation accelerating the migration of point defects. In turn, the extra capacitive time constant was identified as corresponding to an interfacial charge transfer reaction.
4. The parameter estimates obtained from a quantitative comparison of the current vs. potential curve and impedance spectra at several potentials with the model equations are in reasonable agreement with values both for the oxide film on Fe in different electrolytes and a range of metals in acidic solutions.

References

1. Vetter K (1971) *Electrochim Acta* 21:1923–1937
2. Macdonald DD (1992) *J Electrochem Soc* 139:3434–3449
3. Macdonald DD (1999) *Pure Appl Chem* 71:951–978
4. Bojinov M, Fabricius G, Laitinen T, Mäkelä K, Saario T, Sundholm G (2000) *Electrochim Acta* 45:2029–2048
5. Bojinov M, Laitinen T, Mäkelä K, Saario T (2001) *J Electrochem Soc* 148:B243–B250
6. Goad D, Dignam M (1972) *Can J Chem* 50:3259–3266
7. Goad D, Dignam M (1972) *Can J Chem* 50:3267–3271
8. Taylor D, Dignam M (1973) *J Electrochem Soc* 120:1299–1305
9. De Wit H, Wijenberg C, Crevecoeur C (1979) *J Electrochem Soc* 126:779–785
10. Young L, Smith D (1983) *J Electrochem Soc* 130:408–412
11. Kirchheim R (1989) *Corros Sci* 29:183–190
12. Kluger K, Lohrengel M (1991) *Ber Bunsenges Phys Chem* 95:1458–1461
13. Lohrengel M (1993) *Ber Bunsenges Phys Chem* 97:440–447
14. Keddad M, Lizée J-F, Pallotta C, Takenouti H (1984) *J Electrochem Soc* 131:2016–2024
15. Gabrielli C, Keddad M, Minouflet F, Perrot H (1996) *Electrochim Acta* 41:1217–1222
16. Young L, Yang T, Backhouse C (1995) *J Electrochem Soc* 142:3479–3483
17. Young L, Yang T, Backhouse C (1995) *J Electrochem Soc* 142:3483–3485
18. Biaggio S, Rocha Filho R, Vilche J, Varela F, Gassa L (1997) *Electrochim Acta* 42:1751–1758
19. Li Y, Young L (1998) *Electrochim Acta* 44:605–611
20. Li Y, Young L (1998) *Proc R Soc A* 454:239–246
21. Li Y, Young L (2000) *J Electrochem Soc* 147:1344–1348
22. Frateur I, Cattarin S, Musiani M, Tribollet B (2000) *J Electroanal Chem* 482:202–210
23. Cattarin S, Musiani M, Tribollet B (2002) *J Electrochem Soc* 149: B457–B464
24. Wu H, Hebert K (2002) *Electrochim Acta* 47:1373–1383
25. Jonscher A (1986) *J Chem Soc Faraday Trans 2*(82):75–81
26. Beale M (1992) *Phil Mag B* 65:65–77
27. Bojinov M (1997) *Electrochim Acta* 42:3489–3497
28. Bojinov M, Fabricius G, Laitinen T, Saario T (1999) *Electrochim Acta* 44:4331–4343
29. Bojinov M, Cattarin S, Musiani M, Tribollet B (2003) *Electrochim Acta* 48:4107–4117
30. Karastoyanov V, Bojinov M (2008) *Mater Chem Phys* 112:702–710
31. Karastoyanov V, Bojinov M (2009) *J Solid State Electrochem* 13: 309–320
32. Bojinov M, Karastoyanov V, Tzvetkov B (2010) *ECS Trans* 25:89–104
33. Stancheva M, Bojinov M (2012) *Electrochim Acta* 78:65–74
34. Stancheva M, Bojinov M (2013) *J Solid State Electrochem* 17:1271–1283
35. Davenport A, Oblonsky L, Ryan M, Toney M (2000) *J Electrochem Soc* 147:2162–2173
36. Bojinov M, Betova I, Fabricius G, Laitinen T, Raicheff R (1999) *J Electroanal Chem* 475:58–65
37. Peat R, Peter L (1987) *J Electroanal Chem* 228:351–364
38. Abrantes L, Peter L (1983) *J Electroanal Chem* 150:593–601
39. Searson P, Latanision R, Stimming U (1988) *J Electrochem Soc* 135: 1358–1363
40. Burleigh TD (1989) *Corrosion* 45:464–472
41. Piazza S, Sperandeo M, Sunseri C, Di Quarto F (2004) *Corros Sci* 46: 831–851
42. Santamaria M, Terracina S, Konno Y, Habazaki H (2013) *Di Quarto F* 17:3005–3014

43. Oblonsky L, Davenport A, Ryan M, Isaacs H, Newman R (1997) *J Electrochem Soc* 144:2398–2404
44. Schroeder V, Devine T (1999) *J Electrochem Soc* 146:4061–4070
45. Oblonsky L, Ryan M, Isaacs H (2000) *Corros Sci* 42:229–241
46. Albu C, Van Damme S, Abodi L, Demeter A, Deconinck J, Topa V (2012) *Electrochim Acta* 67:119–126
47. Sharifi-Asl S, Taylor M, Lu Z, Engelhardt G, Kursten B, Macdonald DD (2013) *Electrochim Acta* 102:161–173